View metadata, citation and similar papers at core.ac.uk

brought to you by CORE

provided by Open Archive Toulouse Archive Ouverte

Open Archive Toulouse Archive Ouverte (OATAO)

OATAO is an open access repository that collects the work of some Toulouse researchers and makes it freely available over the web where possible.

This is an author's version published in: https://oatao.univ-toulouse.fr/22814

Official URL: https://doi.org/10.2514/1.J057985

To cite this version :

Aguirre, Miguel A. and Duplaa, Sébastien Exergetic Drag Characteristic Curves. (2019) AIAA Journal. 1-12. ISSN 0001-1452

Any correspondence concerning this service should be sent to the repository administrator: tech-oatao@listes-diff.inp-toulouse.fr

Exergetic Drag Characteristic Curves

Miguel A. Aguirre[1] and Sébastien Duplaa[2]
ISAE SUPAERO - Institut Supérieur de l'Aéronautique et de l'Espace, Toulouse, 31055, France

This paper aims to perform a drag breakdown of an airfoil and a wing by using the exergetic method. Moreover, a new far-field wave anergy extraction method is presented. The resulting exergetic drag curves are proposed as additional characteristic curves for external aerodynamic assessment of airfoils or any other bodies. CFD analyses of a NACA 0012 airfoil and a rectangular wing at subsonic and transonic conditions were used as test cases to present the concept. This new approach allows to deeply understand the aerodynamic behavior of a body and provides an alternative point of view to the classical near-field and far-field based drag curves.

Nomenclature

$\dot{\mathcal{A}}$ = total anergy outflow rate, W

$\dot{\mathcal{A}}_{\Phi}$ = viscous anergy rate created inside the control volume, W

$\dot{\mathcal{A}}_{\nabla T}$ = thermal anergy rate, W

$\dot{\mathcal{A}}_{w}$ = shockwave anergy rate, W

a = speed of sound, $m.s^{-1}$

α = angle of attack, Degrees

C_D = drag coefficient

c = airfoil chord, m

c_p = mass specific heat at constant pressure, $J.kg^{-1}.K^{-1}$

D = drag force, N

$\delta(\ )$ = $(\ ) - (\ )_0$, local variation of a parameter respect to the upstream value

[1] Research and development engineer, DAEP-Department of Aerodynamics, Energetics and Propulsion; Miguel-angel.AGUIRRE@isae-supaero.fr.
[2] Associate professor, DAEP-Department of Aerodynamics, Energetics and Propulsion; Sebastien.DUPLAA@isae-supaero.fr.

$\dot{E}_u$ = axial kinetic energy outflow rate, W

$\dot{E}_v$ = transverse kinetic energy outflow rate, W

$\dot{E}_p$ = boundary-pressure work rate, W

e = mass specific internal energy, J.kg^{-1}

$\dot{\varepsilon}_{prop}$ = rate of exergy supplied by the engine, W

$\dot{\varepsilon}_q$ = rate of heat exergy supplied by conduction, W

$\dot{\varepsilon}_m$ = mechanical exergy outflow rate across the survey plane, W

$\dot{\varepsilon}_{th}$ = thermal exergy outflow rate, W

Φ_{eff} = effective dissipation, J.s^{-1}.m^{-3}

Γ = weight specific aircraft energy height, m

γ = ratio of specific heats

h_t = mass specific total enthalpy, J.kg^{-1}

$\boldsymbol{i, j, k}$ = unit vectors along the aerodynamic x-, y- and z-axes

k_{eff} = Fourier law's coefficient

M = Mach number ($= u_0/a_0$)

μ, μ_t = laminar and turbulent dynamic viscosities, kg.m.s^{-1}

$\boldsymbol{n}$ = n_x **i**, n_y **j**, n_z **k**, local surface normal

P_s, P_t = static and total pressure, Pa

Pr = Prandtl number ($= c_p \mu / k$)

Re = Reynolds number ($= \rho_0 \, u_0 \, c / \mu_0$)

ρ = air density, kg.m^{-3}

S = surface, m^2

s = mass specific entropy, J.kg^{-1}.K^{-1}

T_s, T_t = static and total temperatures, K

$\bar{\bar{\tau}}$ = viscous stress tensor, Pa

$\boldsymbol{V}$ = u**i**, v**j**, w**k**, local velocity vector, m.s^{-1}

Subscripts

0 = Upstream values

b = body

ref = reference

I. Introduction

THE characteristic curves of airfoils, wings and any other body are classically obtained by near-field and far-field methods. These methods have been used since longtime and provide a good insight into the physics, thus, they have become a standard for both the industry and the research domains. However, new aerodynamic tools have been developed the last years, where ones of the most promising methods are the Power Balance [1] and the exergy analysis [2]. These two approaches have been extensively used for the performance assessment of future aircraft configurations like boundary layer ingestion designs [3], where the classical near-field and far-field methods are no longer reliable. Moreover, it provides an alternative analysis for classical configurations, which can be compared against the existing aircraft performance metrics [Hayes-1]. One of the major assets of these methods is their powerful insight into the physics. As a matter of fact, the bodies are studied following a very intuitive mechanical/energetic approach, which leads to a more complete drag breakdown for unpowered cases (and powered cases as well) compared to the classical methods.

In spite of the inherent advantages offered by these methods, they are not currently used to provide the aerodynamic characteristic curves of unpowered bodies (standard airfoil, wing and so on). As a consequence, this work aims to explore this possibility, highlighting its usefulness and potentials, but specially to propose it as a complementary characteristic curve when a standard aerodynamic assessment is performed.

Given that the exergy method is considered as a generalization of the Power balance, only the Exergy Method will be discussed here, but the results are also valid for the Power Balance method.

II. Review of the aerodynamic assessment methods

A. System of reference

The reference system used hereafter is shown in Fig. 1. It has the x-axis aligned with the upstream flow direction and pointing rearwards, the y-axis points towards the right-hand side of the body and the z-axis points upwards. Moreover, when control volume formulations are used, it is assumed that the outlet section “Sout” of the control

volume is a plane (called "survey plane") and it is placed normal to the x-axis. Also, the lateral surfaces are considered parallels to the upstream direction and far away from the body.

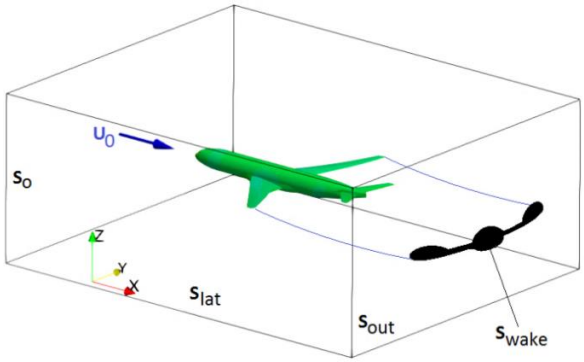

Fig. 1 Conventional reference frame.

B. Near-field method

The most used method to obtain the total drag force "D" acting upon a body is the near-field method [4,5].

$$D = \int_{S_b} (P_s \, \overrightarrow{n_x} - \bar{\bar{\tau}} \, . \overrightarrow{n_x}) \, dS_b \tag{1}$$

This approach has the advantage to be very simple and easy to understand. However it only allows to decompose the drag into its pressure and friction components, which does not give a complete comprehension of the physics: this highlights its drawbacks for design analysis purposes.

C. Far-field method

A more powerful aerodynamic assessment can be done by using the so-called far-field methods. All of them apply the momentum conservation equation to a control volume surrounding the body in order to define a set of equations allowing a phenomenological decomposition of drag, while giving at the same time a good insight into the physics. Several variants of this method are available [6-9] allowing the extraction of the drag force by only analyzing the wake of a body, but here we will discuss only the most recent approach for wind tunnel measurement of stationary flows [10]. It is based on the small perturbations method and the decomposition of the axial velocity deficit inside the wake. This leads to the following profile drag equation which is valid for compressible and incompressible regimes:

$$D_{profile} = \frac{\rho_0 \, {u_0}^2}{2} \int_{S_{wake}} \left[-\frac{2}{\gamma \, {M_0}^2} \Delta P_t \; - \Delta T_t + \left(1 - \frac{{M_0}^2}{4}\right) \Delta {T_t}^2 - \Delta P_t \, \Delta T_t - \left(1 - {M_0}^2\right)\left(\Delta \bar{u}^2 + 2 \, \Delta u^* \, \Delta \bar{u}\right) \right] dS \tag{2}$$

Where:

$$\Delta Pt = \frac{P_t}{P_{t_0}} - 1 \tag{3}$$

$$\Delta Tt = \frac{T_t}{T_{t_0}} - 1 \tag{4}$$

$$\Delta u = \frac{u}{U_0} - 1 \tag{5}$$

$$\Delta u^* = \sqrt{1 - \frac{2}{(\gamma-1)\,M_0{}^2}\left(\left(\frac{P_s}{P_{s_0}}\right)^{\frac{(\gamma-1)}{\gamma}} - 1\right) - \frac{v^2+w^2}{U_0{}^2}} - 1 \tag{6}$$

$$\Delta\bar{u} = \Delta u - \Delta u^* \tag{7}$$

The "small perturbation" assumption considers that the variations of total pressure ΔPt, total temperature ΔTt and velocity Δu are small (however, it proved to be also valid for high-lift configurations where the perturbations are not small). Moreover, the velocity perturbation Δu is decomposed into a viscous contribution $\Delta\bar{u}$ (which is null outside the wake) and other component Δu^* related to the potential field.

For 2D applications, the profile drag is the total drag acting upon a body (which includes the viscous drag and the wave drag as it will be shown later). For 3D cases, the vortex drag must also be considered:

$$D_{vortex} = \int_{S_{out}} \frac{\rho}{2}(v^2 + w^2)\, dS \tag{8}$$

$$D_{total} = D_{profile} + D_{vortex} \;\; = D_{viscous} + D_{wave} + D_{vortex} \tag{9}$$

In this study, the survey plane position used for the evaluation of the far-field drag values was placed at 1 chord downstream of the airfoil or wing.

D. Exergy method

The most recent method of drag extraction has been developed by using the exergy approach. This is a classical thermodynamic concept based on the 1st and 2nd laws of thermodynamics [11,12]. It decomposes the total energy of a system into two components: the exergy "ε" (the useful part of the energy) and the anergy "$\mathcal{A}$" (its useless part). The exergy concept states that any perturbation of the system (perturbation of speed, pressure, and so on) can be returned to its original (equilibrium) state by means of a reversible transformation. So, any perturbation has an inherent energetic potential (exergy) that can be converted into work by a reversible transformation. This can be expressed as follows:

$$\varepsilon = \delta h_t - T_{s_0}\,\delta S = \delta h_t - \mathcal{A} \tag{10}$$

Several authors have used this concept to evaluate the external aerodynamic behavior of flight vehicles [13-16]. One of the most recent formulations is the one proposed by Arntz [2]: an exergy approach well adapted for the analysis of CFD simulations and valid for compressible and incompressible flows.

$$\dot{\varepsilon}_{prop} + \dot{\varepsilon}_q = W\dot{I} + \dot{\varepsilon}_m + \dot{\varepsilon}_{th} + \dot{\mathcal{A}}_\Phi + \dot{\mathcal{A}}_{\nabla T} + \dot{\mathcal{A}}_w \tag{11}$$

Each term on the right-hand side represents an equation itself as indicated as follows, where "S_{wave}" is the surface enclosing the shockwave and "sw_{vol}" is the shockwave volume:

$$\dot{\varepsilon}_m = \underbrace{\int_{Sout} \frac{1}{2}\rho\, \delta u^2 (\vec{V}.\vec{n}) dS}_{\dot{E}_u} + \underbrace{\int_{Sout} \frac{1}{2}\rho (v^2 + w^2)(\vec{V}.\vec{n}) dS}_{\dot{E}_v} + \underbrace{\int_{Sout} (P_s - P_{s_0})[(\vec{V} - \vec{V}_0).\vec{n}] dS}_{\dot{E}_p} \tag{12}$$

$$\dot{\varepsilon}_{th} = \int_{Sout} \rho\, \delta e\, (\vec{V}.\vec{n})\, dS + \int_{Sout} P_{s_0} (\vec{V}.\vec{n})\, dS - \underbrace{T_{s_0} \int_{Sout} \rho\, \delta s\, (\vec{V}.\vec{n})}_{\dot{\mathcal{A}}} dS \tag{13}$$

$$\dot{\mathcal{A}}_\Phi = \int_v \frac{T_{s_0}}{T_s} \Phi_{eff}\, dv \tag{14}$$

$$\dot{\mathcal{A}}_{\nabla T} = \int_v \frac{T_{s_0}}{T_s^2} k_{eff}\, (\nabla T)^2\, dv \tag{15}$$

$$\dot{\mathcal{A}}_w = T_{s_0} \int_{S_{wave}} (\rho\, \delta s\, \vec{V}).\vec{n}\ \ dS = \int_{SW_{vol}} \nabla.(T_{s_0}\, \rho\, \delta s\, \vec{V})\ \ dsw_{vol} \tag{16}$$

$$\kappa_{eff} = c_p \left(\left(\frac{\mu}{Pr}\right) + \left(\frac{\mu_t}{Pr_t}\right) \right) \tag{17}$$

$$\Phi_{eff} = (\bar{\bar{\tau}}.\nabla).\vec{V} \tag{18}$$

The mechanical exergy outflow rate $\dot{\varepsilon}_m$ represents the amount of mechanical power that can be recovered by a suited exergy recovery system (e.g., BLI). It is related to the axial and transverse velocity field perturbations ($\dot{E}_u$ and $\dot{E}_v$ respectively) and the pressure field perturbations $\dot{E}_p$. The thermal exergy $\dot{\varepsilon}_{th}$ represents the amount of thermal energy that can be recovered. If the exergies are not valued (recovered) they will be gradually destroyed downstream, becoming a loss. On the other hand, the total anergy $\dot{\mathcal{A}}$ represents the total amount of energy that has been already lost by the system (quantified by the entropy increase). It can be decomposed into the viscous losses $\dot{\mathcal{A}}_\Phi$, the thermal losses $\dot{\mathcal{A}}_{\nabla T}$ and the shockwave losses $\dot{\mathcal{A}}_w$ (if any). Please note that viscous and thermal anergy creation takes place inside the boundary layer but also inside the wake. The terms on the left-hand side represent the sources of exergy, thus the difference between the sources and the losses (given by the anergy and the exergy –if its

potential is not valued-) drives the "$W\dot{I}$" term. This term represents the rate of change in energy height of the body (i.e., potential or kinetic energy variation rate). When the sources exceed the losses, an increase of energy height of the body (e.g., an aircraft) is obtained, which represents a gain of altitude or speed.

This exergetic formulation allows obtaining the so-called "exergetic drag coefficient" when an unpowered and adiabatic case is considered. It is given by the following expression, which allows performing a breakdown of the drag coefficient:

$$C_{D_\varepsilon} = \frac{\dot{\varepsilon}_m + \dot{\varepsilon}_{th} + \dot{\mathcal{A}}_\Phi + \dot{\mathcal{A}}_{\nabla T} + \dot{\mathcal{A}}_w}{\frac{1}{2}\rho_0 \, {U_0}^3 \, S_{ref}} \tag{19}$$

Please note that the exergetic drag coefficient is proportional to the "$W\dot{I}$" term, thus a variation of the drag coefficient can also be interpreted as variation of its energy height.

On the other hand, the drag, exergy and anergy values will be adimensionalized by following the classical approach:

$$C_D = \frac{\mathrm{D}}{\frac{1}{2}\rho_0 \, {u_0}^2 \, S_{ref}} \tag{20}$$

$$C\dot{\varepsilon} = \frac{\dot{\varepsilon}}{\frac{1}{2}\rho_0 \, {u_0}^3 \, S_{ref}} \tag{21}$$

$$C\dot{\mathcal{A}} = \frac{\dot{\mathcal{A}}}{\frac{1}{2}\rho_0 \, {u_0}^3 \, S_{ref}} \tag{22}$$

The drag coefficient values will be presented in drag counts, defined as one ten thousandth of C_D (1dc = 0.0001 C_D). The exergy-based drag coefficient will be displayed in "power counts" (pc), defined as one tenth thousandth of "C_{D_ε}", i.e., 1pc = 0.0001 C_{D_ε} (The same applies for the exergy/anergy coefficients). Indeed, the exergy-based drag coefficient is equivalent to the force-based drag coefficient, thus, the power counts and drag counts units will be used interchangeably.

The terminology and notation of the exergetic method is not completely standardized yet [2]. In particular, "Anergy" represents the so-called "exergy destruction" in the fluid dynamics domain [Hayes-2] (moreover, it has another different meaning in the medical field [xx]). Thus, the usage of the word "anergy" seems to be redundant. However, it will be used "anergy" as synonym of "exergy destruction" throughout this paper in order to be in line with the nomenclature introduced by Arntz whose work is intended to be deepened here.

III. CFD data

In order to evaluate the different drag extraction methods, CFD data will be used. The 2D case is a NACA 0012 airfoil with sharp trailing edge. The 3D case is a rectangular wing of aspect ratio 8 with the same airfoil and rounded wing tip. In both cases a C-block structured grid with wake refinement was used (See Fig. XX). The domain extent was 150 chords in all directions for the 2D case and 30 chords for the 3D case. For the 2D case, a grid refinement was performed and the near-field drag value compared against experimental data of the bibliography [xxx] as shown in Fig.XX. Then the mesh of 593.000 cells was selected for the 2D case, which ensured the correct capture of all the physical phenomena even in transonic condition. For the 3D case, a coarser mesh (adapted for subsonic cases only) was extruded spanwise obtaining a 9.2 million cells mesh. The mesh blocking and refinement on the wake region was different for each angle of attack for both 2D and 3D meshes: the refinement zone follows the wake deviation in order to ensure a proper capture of the wake.

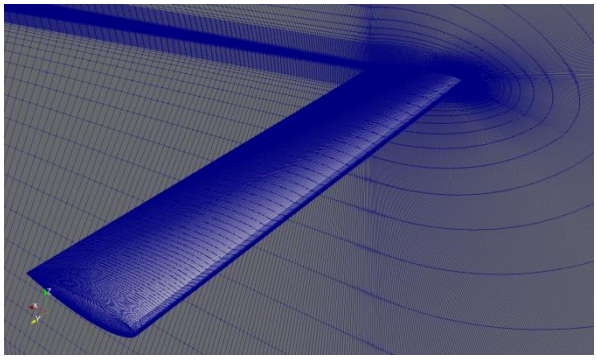

Fig. 2 3D mesh for α=0°

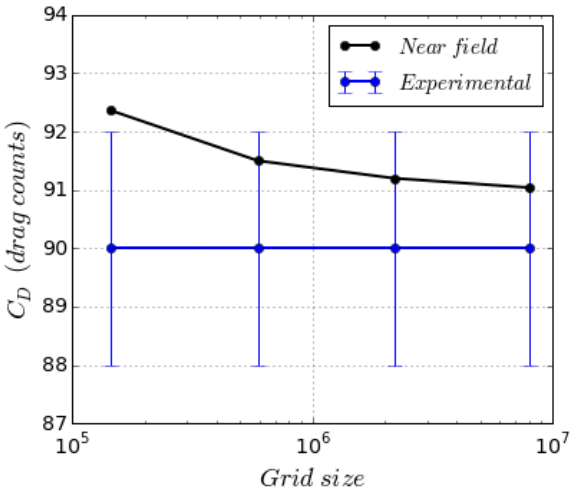

Fig. 3 Grid convergence for α=0°, M=0.3 and Re=3.10^6

The 2D and 3D cases have been analyzed for several angles of attack at constant Mach number of 0.3 and Reynolds number of 3.10^6. Moreover, the 2D case was also analyzed at several Mach number with fixed angle of attack (0°). In all the cases the RANS simulations were performed with Spalart Allmaras turbulence model. A first quick convergence was done with a first-order discretization for flow and turbulence by about 3000 iterations, followed by a final second-order discretization convergence as shown in Fig. XX. All the simulations were left running until the near-field drag coefficient varies less than 0.1 drag counts from one iteration to the following. At the same time, it was verified that the residuals reached the maximum precision in order to ensure that the airfoil losses information is completely transmitted (convected) downstream. Then, the y^+ parameter was controlled in order to verify that $y^+ \leq 1$ everywhere around the body (as required by the Spalart Allmaras model). The resulting CFD data was analyzed with a Paraview's plugin called Epsilon, which allows performing a far-field and exergetic analysis. Further details on the grids, solver setup and the post-processing code is available in Ref. [17], including the CFD data validation.

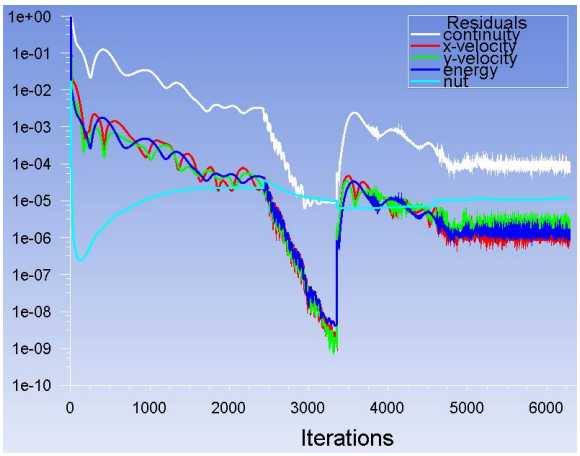

Fig. 4 Residuals convergence for the airfoil at α=0°/M=0.3

IV. Airfoil/wing exergetic-based characteristic curves

First the 2D cases will be analyzed to introduce the methodology. Then it will be extended to the 3D cases.

A. NACA 0012 airfoil

The three drag extraction methods are compared in Fig. 2, where the typical airfoil drag curve is shown (The exact values are also provided in Table 1). The near-field values are provided by the CFD RANS solver itself (Fluent) and it will be used as a reference to evaluate the other two methods (Far-field and exergy). The far-field

method was implemented by using a survey plane placed at 1 chord downstream of the airfoil (a standard practice). On the other hand, the exergetic analysis was implemented at two survey planes: one placed at the trailing edge (TE) and the other one placed 1 chord downstream of the trailing edge (1C). It can be seen that the drag values of the four methods matches very well. This comparison gives confidence in the results so now we can go deeply into our main objective: the drag breakdown analysis.

Table 1 drag coefficient values (drag counts)

α (°)	Near-field	Far-field	Exergy TE	Exergy 1C
0	91.58	91.12	92.50	91.80
2	93.41	92.74	94.13	93.51
4	99.08	98.14	98.93	98.03
6	109.45	108.06	107.58	106.76
8	126.2	124.31	126.69	125.48
10	154.07	151.53	155.16	153.97

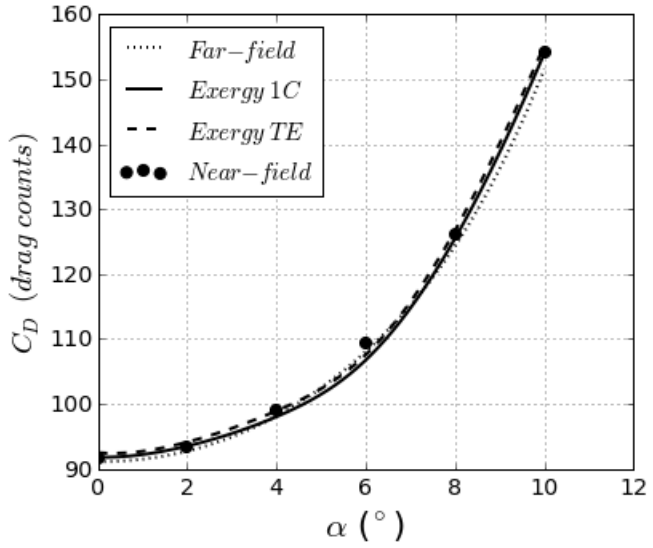

Fig. 2 Airfoil drag coefficient extraction by several methods

Firstly, the classical near-field method will be analyzed: its drag coefficient breakdown can be shown on the Fig. 3. This formulation only allows decomposing the drag coefficient into its pressure and friction components. It can be seen that the increase of profile drag with the angle of attack is directly linked to the increase of its pressure component. This is mainly related to the x-component of the rear upper surface total suction force that becomes intense at high angles of attack. On the other hand, the friction component tends to decrease with the angle of attack because the local velocities are being reduced (compared to the 0° angle of attack case) on the lower surface and the

rear part of the upper surface, reducing the local skin friction magnitude. Nevertheless, this drag breakdown is not very useful for airfoil design purposes: a further insight into the physics would be desirable.

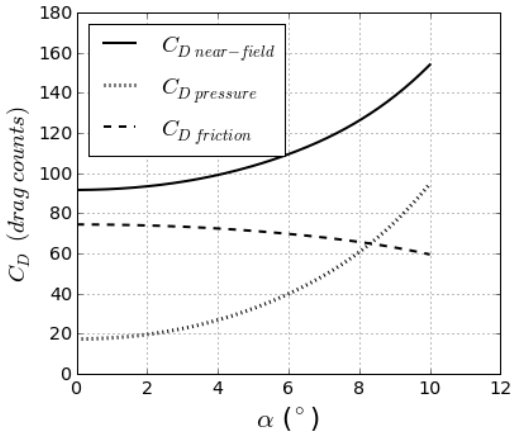

Fig. 3 Near-field drag breakdown

The alternative approach is the far-field method. In its classical incompressible 2D application, no further breakdown is possible as it is shown in Fig. 4. This method takes advantage of its formulation on 2D transonic cases (where the drag can be decomposed into wave drag and profile drag) or even better, on 3D cases (where also the vortex drag can be extracted from the total drag). Even though the far-field formulation may allow a term-by-term analysis to perform a related "breakdown", this approach is challenging because the formulation contains several second order mathematical terms (obtained from the small perturbations approach) whose physical analysis is not direct at all. This problem is solved in a very proper fashion by the exergetic analysis.

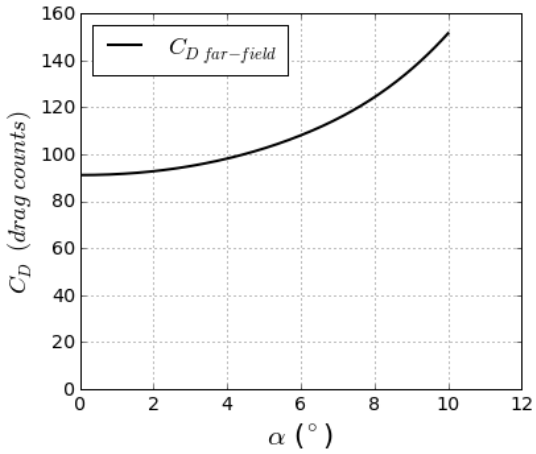

Fig. 4 Far-field drag breakdown

One of the major advantages of the exergetic analysis is that every single term of its formulation has a clear and easy to understand physical meaning. Thus, using its terms to perform a drag breakdown is straightforward as it is

shown in the Fig. 5, where the classical airfoil profile drag curve was decomposed into its three main components: the total anergy "$\dot{\mathcal{A}}$", the mechanical exergy "$\dot{\varepsilon}_m$" and the thermal exergy "$\dot{\varepsilon}_{th}$".

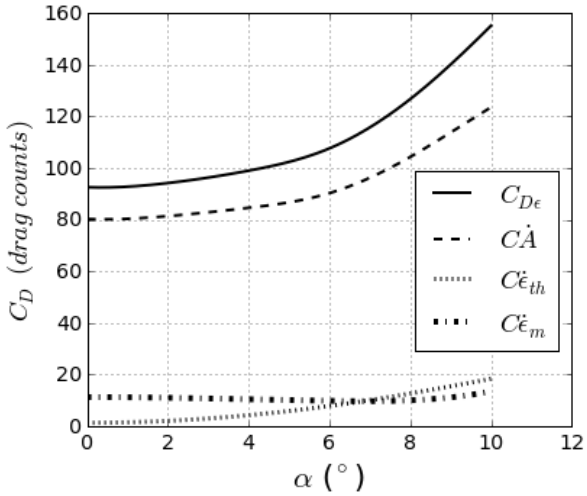

Fig. 5 Exergetic drag breakdown

The total anergy represents the part of the airfoil's work potential that has been destroyed by viscous dissipation, turbulence and thermal mixing inside the boundary layer (irreversible processes). Thus, this rate of energy loss is perceived a drag contribution. The behavior of its curve is easy to understand. As a matter of fact, it is known that the boundary layer size and its local strain increase with the angle of attack, leading to an increase of the viscous and thermal losses inside the boundary layer. That's why the total anergy increases with the angle of attack. In turn, this total anergy curve can also be decomposed into its pure viscous and thermal components as shown in Fig. 6, where the same curve behavior is found for both components, and where it is seen that the viscous anergy is predominant.

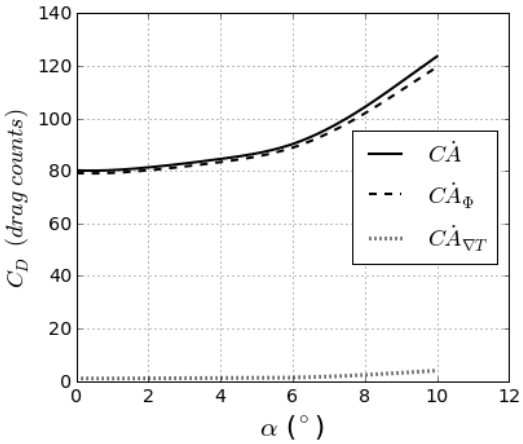

Fig. 6 Anergy breakdown

The thermal exergy outflow of the Fig. 5 represents the thermal energy perturbation flowing out of the domain and that it is not being recovered as work (by theoretically using a Carnot cycle). Its work potential is simply being

lost and thus its waste of energy becomes as a drag component. As the thermal effect takes place mainly inside the boundary layer, it is clear that this drag component increases with the angle of attack.

On the other hand, the mechanical exergy outflow of Fig. 5 represents the total mechanical energy perturbations (kinetic and pressure energies) with respect to the equilibrium conditions (the upstream condition) that are created by the airfoil and being lost across the survey plane. As the airfoil must use its energy height to compensate the energy consumed by such perturbations (for an unpowered/adiabatic flight), the mechanical exergy outflow is perceived as another drag component. This can be further decomposed into its axial and transverse kinetic energies components and the boundary-pressure work rate as shown in Fig. 7. "E_u" is mainly related to the axial kinetic energy variation inside the wake (associated to the wake velocity deficit) which increases with the angle of attack. In 2D cases, "E_v" is mainly related to the flow deviation by the airfoil circulation (thus related to the airfoil's lift), which also increases with the angle of attack. "E_p" is mainly related to the pressure deficit inside the wake which varies with the angle of attack. Its negative sign is due to the fact that the velocity deficit inside the wake is negative (local velocity smaller than free-stream velocity). Those three terms are coupled by velocity-pressure mechanism, that's why they are grouped into the net total mechanical exergy outflow term "E_m". Special attention must be addressed to the "E_p" term because its negative value could be interpreted as a thrust, however it is nothing but the pressure perturbation linked to the velocity perturbation. Even though both perturbations (pressure and velocity) represent an important amount of drag counts, the only useful (recoverable) part is the mechanical exergy: this parameter already takes into account the compensation of its terms (velocity-pressure mechanism).

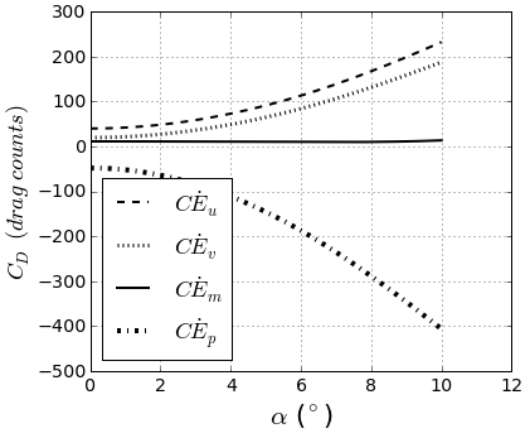

Fig. 7 Mechanical exergy outflow rate breakdown

From this analysis it can be seen that the exergetic method allows obtaining a far more complete and intuitive airfoil drag breakdown, giving place to a new family of characteristic curves for an airfoil: the exergetic

characteristic curves. Even though this method was developed mainly for the analysis of coupled aircraft configurations, it would be extremely useful to implement it for airfoil design purposes and to provide a more complete airfoil performance assessment. For example, laminar airfoils performance is often presented by using the classical profile drag characteristic curve. However, the exergetic breakdown will allow to clearly quantify the change in viscous anergy due to transition delay from one airfoil design to another. This highlights the power of this approach for airfoil design purposes.

The survey plane used on the previous exergy analysis is placed at the trailing edge of the airfoil. At this position a maximum amount on exergy can be recovered (this is supported by early incompressible studies [xxx]). Other surveys planes could also be used but the exergetic components will be redistributed because they are plane position-dependent. Moreover, for the positions downstream of the trailing edge some wake exergy has been already destroyed and converted into anergy, distorting the perception of the airfoil's behavior.

So far we have discussed about the classical airfoil drag curve vs angle of attack. We will now go forward to analyze the C_D vs Mach curve as it is shown in Fig. 8 for all the methods already discussed. A general agreement is observed for all the methods, especially on the drag rise region. On the compressible subsonic region there are some small differences, especially for the far-field method (taking always the near-field values as the reference), but the exergetic methods seem to provide more accurate results.

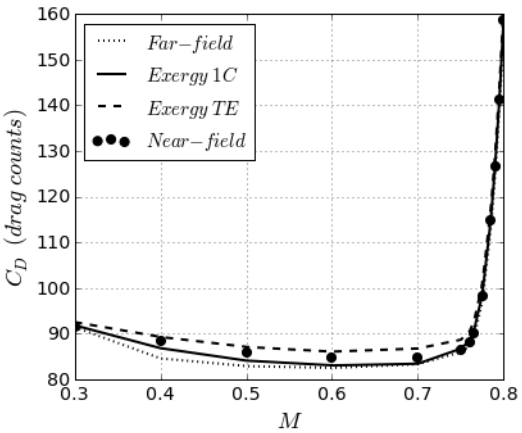

Fig. 8 Airfoil drag coefficient extraction by several methods (α=0°)

As before, a breakdown of the near-field curve is performed in order to show its pressure and friction components as it is seen on Fig. 9. Note that the pressure drag increases with the Mach number on the subsonic range because of the compressibility effects and then it rises because of the shockwave appearance. Again, as in the C_D vs angle of attack curve, the high complexity of the physics is not completely highlighted with this method.

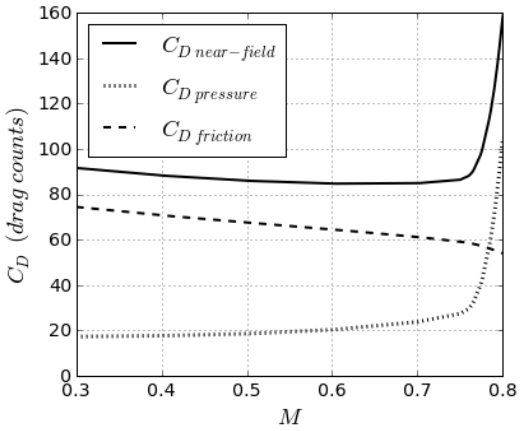

Fig. 9 Near-field drag breakdown

The far-field method allows performing a profile drag breakdown by using the Kusunose approach [18]. It decomposes the profile drag in the transonic range into its pure viscous, pure wave and wave-boundary layer interaction components as shown in the Fig. 10. According to Kusunose, the total wave drag is the sum of the pure wave and the interaction part (this aspect of his approach will be revised later).

As it was expected, the total wave drag is zero on the subsonic zone and it increases very quickly with the Mach number on the transonic range because the shockwave losses become stronger. The pure viscous drag tends to decrease on the transonic region which does not seems to be very representative of the physics because the viscous drag should increase as a consequence of the boundary layer thickening induced by the shockwave (this will also be analyzed in detail later).

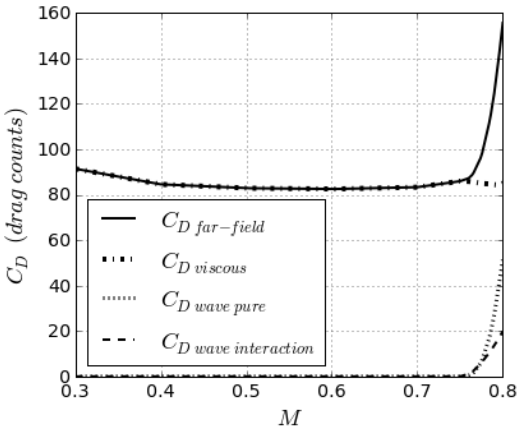

Fig. 10 Far-field drag breakdown

The exergetic drag breakdown is shown in Fig. 11. The total anergy rate presents a sudden increase in the transonic region due to the appearance of the shockwaves, leading to a new anergy component: the wave anergy

"$\dot{\mathcal{A}}_w$" (See Fig. 12). In fact, new losses appear on the shockwave region associated to its non-isentropic process. It means that the airfoil wastes its energy height in order to compensate the energy required to create such irreversible phenomenon (the shockwave): this is perceived as a drag component. On the other hand, the thermal anergy increases with Mach number as expected because thermal effect starts being more intense at high speeds. Moreover, the viscous anergy increases when shockwaves are present because the boundary layer thickens due to the shockwave interaction, increasing its related losses. The thermal exergy outflow rate of the Fig. 11 increases with Mach number as expected (because the thermal boundary layer starts being stronger) but the mechanical exergy decreases and even becomes negative (apparent thrust). This is due to the fact that the boundary-pressure work rate becomes its predominant component at high Mach numbers due to the compressibility effects, as it is shown in Fig. 13. If the survey plane would be placed downstream of the airfoil, this pressure component would not be so strong and the net mechanical exergy would be positive and the "apparent thrust" mentioned before will no longer be present.

The viscous and thermal anergy values shown in Fig. 12 have been corrected following the method proposed by Arntz [2] in such a way that the sum of the viscous (Eq. 14), thermal (Eq.15) and wave (Eq.16) anergies, is equal to the total anergy (Eq. 13).

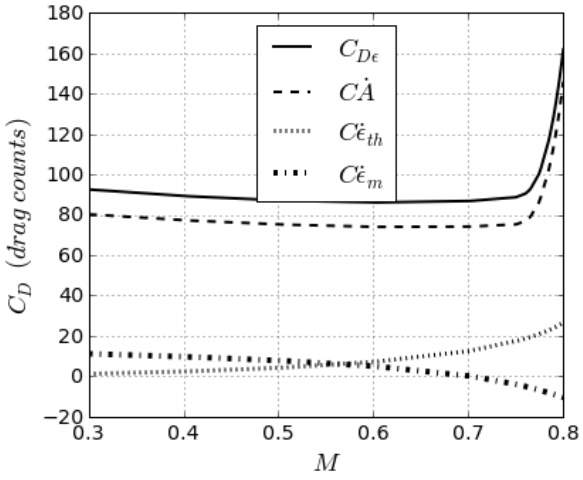

Fig. 11 Exergetic drag breakdown

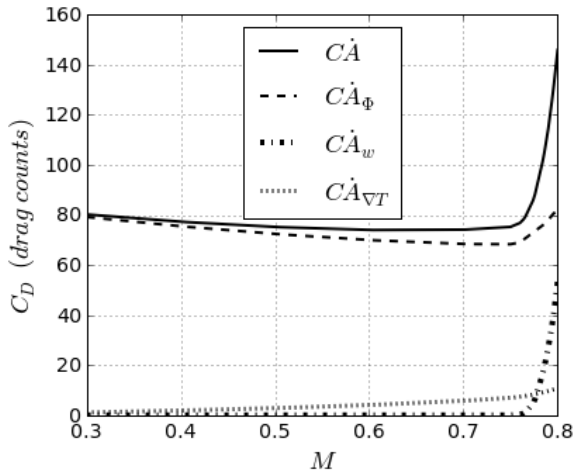

Fig. 12 Total anergy breakdown

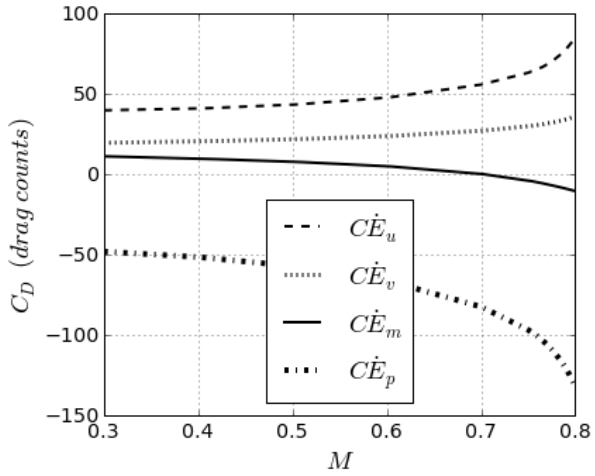

Fig. 13 Mechanical exergy outflow rate breakdown

The results discussed before highlights the fact that the exergetic method offers a simple and intuitive explanation to the compressibility and transonic effects. As it was indicated for the case of the C_D vs angle of attack curve, it would be extremely useful to implement the exergetic analysis to improve the aerodynamic assessment of airfoils or any other body. This does not mean at all that the near-field and far-field methods must be discarded. On the contrary, it is proposed to use the exergetic method as a complementary tool to perform a more complete aerodynamic assessment. As a matter of fact, the near-field, far-field and exergy methods provide different points of view of the same physical phenomena. However, the exergy method offer a completely new way to analyze and understand the flow fields, based on an energetic reasoning rather than a classical mechanical point of view (used on the near-field and far-field methods).

B. Rectangular wing

For the rectangular wing we will follow a similar procedure but we will concentrate our attention this time to the vortex drag and its related transverse kinetic energy. The first step is to compare the three approaches to extract the total drag coefficient of the wing, as shown in Fig. 14, where an excellent match is shown (The exact values are shown in Table 2). Thus we can go into our analysis knowing that the drag values are comparable.

Table 2 drag coefficient values (drag counts)

α (°)	Near-field	Far-field	Exergy TE	Exergy 1C
0	94.61	93.82	96.28	95.68
2	110.58	108.31	109.41	108.94
4	149.43	148.40	148.43	147.65
6	213.66	217.67	213.84	212.91
8	304.08	312.05	305.70	303.73
10	420.28	420.65	424.20	421.44

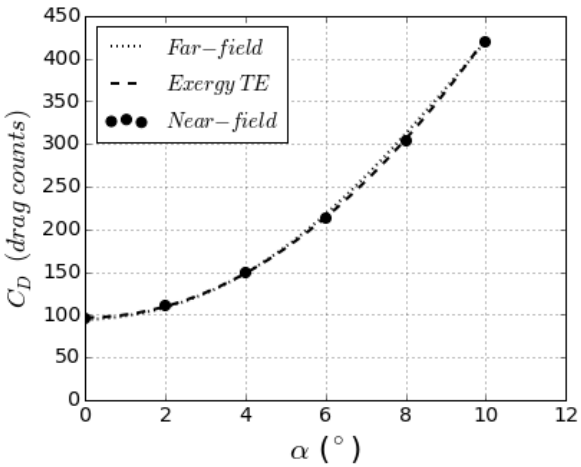

Fig. 14 Wing total drag coefficient extraction by several methods (M=0.3)

Firstly, the classic near-field drag breakdown is done in the Fig. 15. It is clear that the pressure component drives the total drag curve, but it does not put into evidence the existence of the wing tip vortices. Thus, the utility of this breakdown is limited.

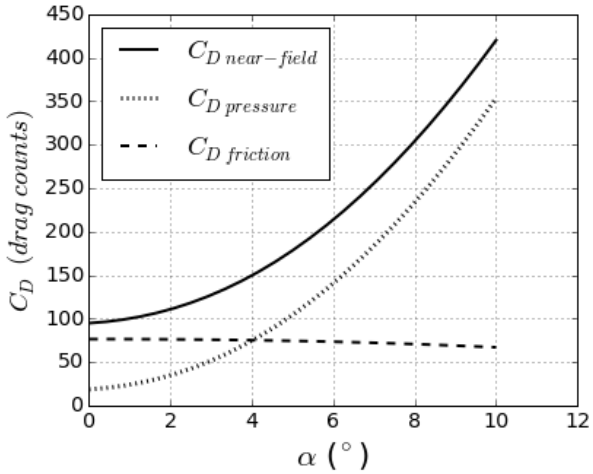

Fig. 15 Near-field drag breakdown

Secondly, the far-field decomposition method is used to obtain the two main components of the total drag as it is shown in Fig. 16. This time, the strengthening of the wing tip vortices (actually, the vortex sheet shed by the wing) with the angle of attack is explicitly displayed. Thus, the physics is better explained with this method.

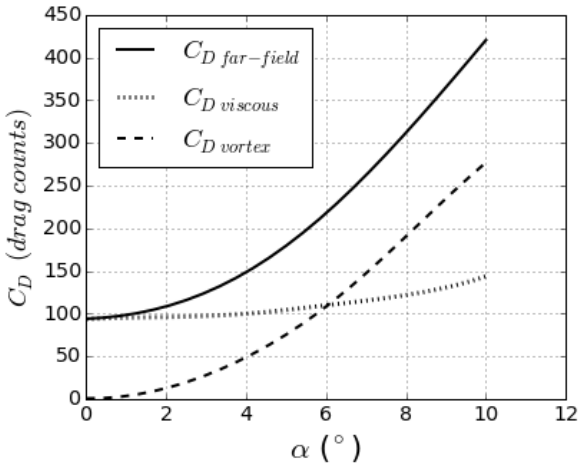

Fig. 16 Far-field drag breakdown

Finally, the exergetic method is used to perform a total drag breakdown as it is shown in the Figs. 17, 18 and 19. In Fig. 17 is clear that the thermal exergy and the total anergy almost did not change from the 2D case. However, the mechanical exergy outflow is showing a significantly increase with the angle of attack. This is because the transverse kinetic energy also increases with the angle of attack (Fig.19). In fact, "E_v" takes into account the "$\frac{1}{2}\rho(v^2 + w^2)$" term which is related to the transverse rotational velocity field associated to the wing tip vortex (vortex drag).

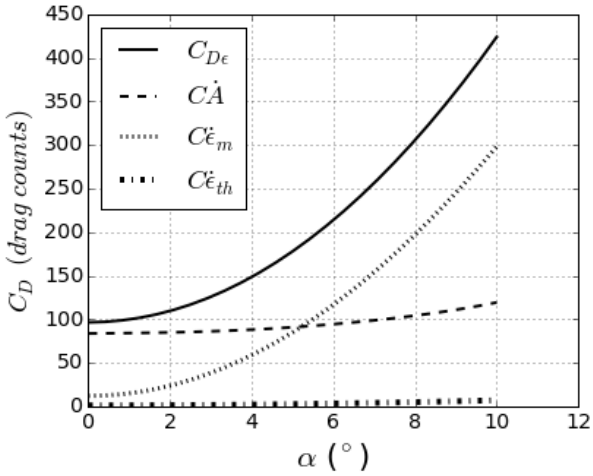

Fig. 17 Exergetic drag breakdown

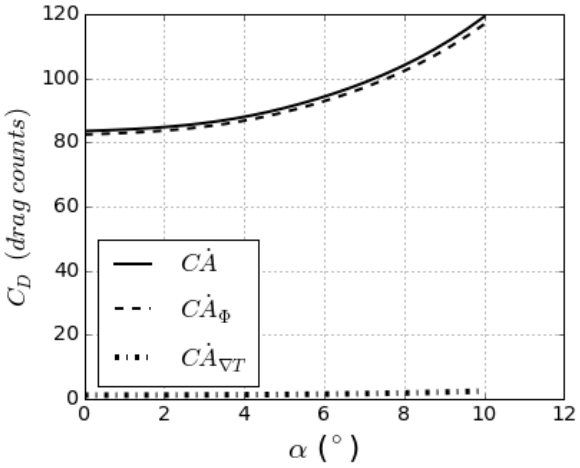

Fig. 18 Total anergy breakdown

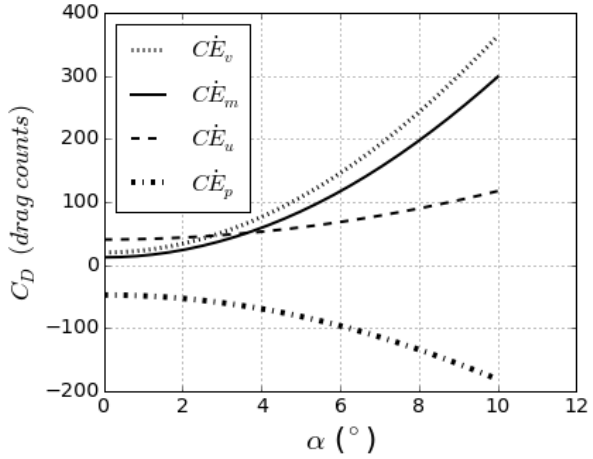

Fig. 19 Mechanical exergy outflow rate breakdown

This 3D study confirms that the exergy approach provides better qualitative and quantitative information for the aerodynamic assessment of a body. Thus, it is advisable to use it as a complement to the standard techniques in order to determine the wing characteristic curves.

V. Far field wave drag/anergy extraction method

As it was indicated before, the far-field wave extraction method proposed by Kusunose presents some inconsistencies so it will be re-studied by using the exergetic method as a physical comprehension support analysis. Moreover, a new far-field wave anergy extraction method will be presented.

A. Kusunose method

The profile drag breakdown proposed by Kusunose [18] uses a physic-based approach to extract the wave drag from the measured profile drag at the survey plane. An example of the profile drag density distribution is shown in the Fig. 20 (by "density" we denote the integrand of its related equation). The colored field corresponds to the Meheut's method drag density at each point, the black line is the survey line and the white line represents the distribution of the drag density along this line. This drag density distribution contains the viscous losses as well as the losses across the shockwave. Note that the pure shockwave losses are convected downstream as it can be seen on the green region. Thus the part of the profile density lying on this zone is precisely the pure wave drag component.

In order to extract this wave component, a physical analysis is done. In fact, the losses across the shockwave are associated to an almost-irotational phenomenon (some small vorticity magnitude is present downstream of the shockwave because of its curvature) however, the viscous losses are related to a strongly rotational phenomena. Hence, a vorticity threshold value is used to define the region of pure wave drag as it is shown in Fig. 21. This allows to decompose the total drag density profile as shown in Fig. 22.

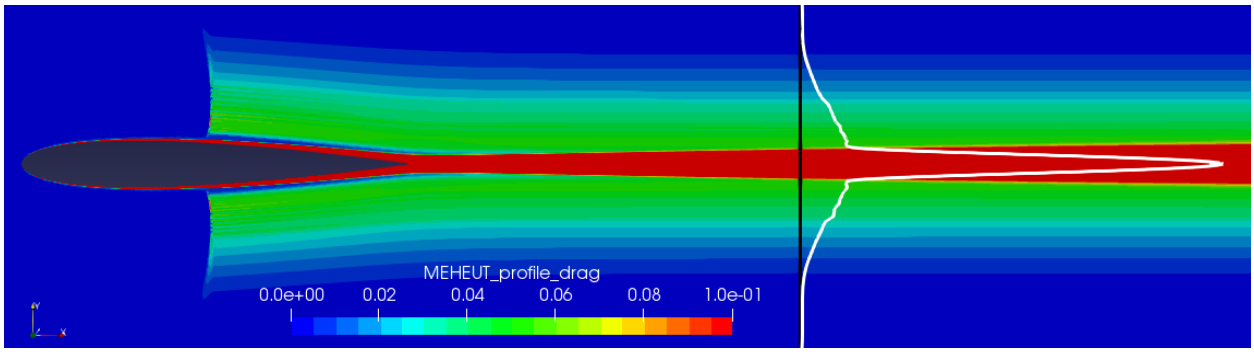

Fig. 20 Drag density field and its distribution along a survey line (M=0.85, α=0°)

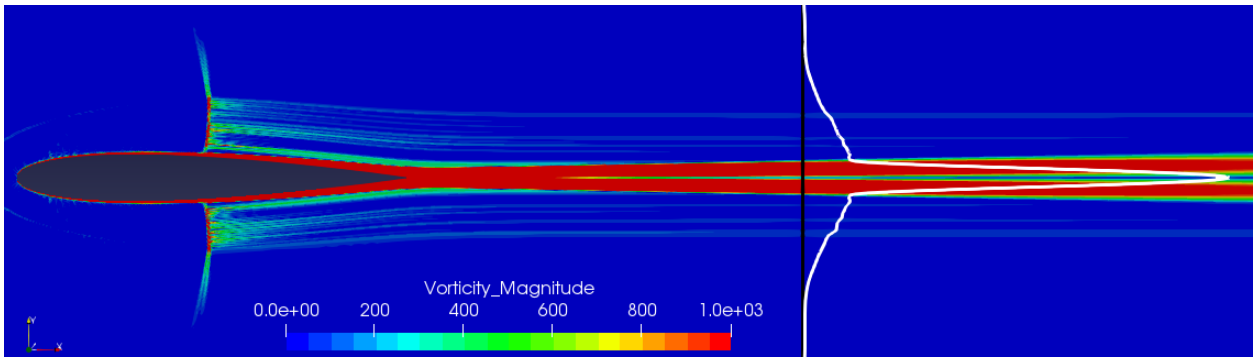

Fig. 21 Vorticity magnitude field and drag density distribution along survey line (M=0.85, α=0°)

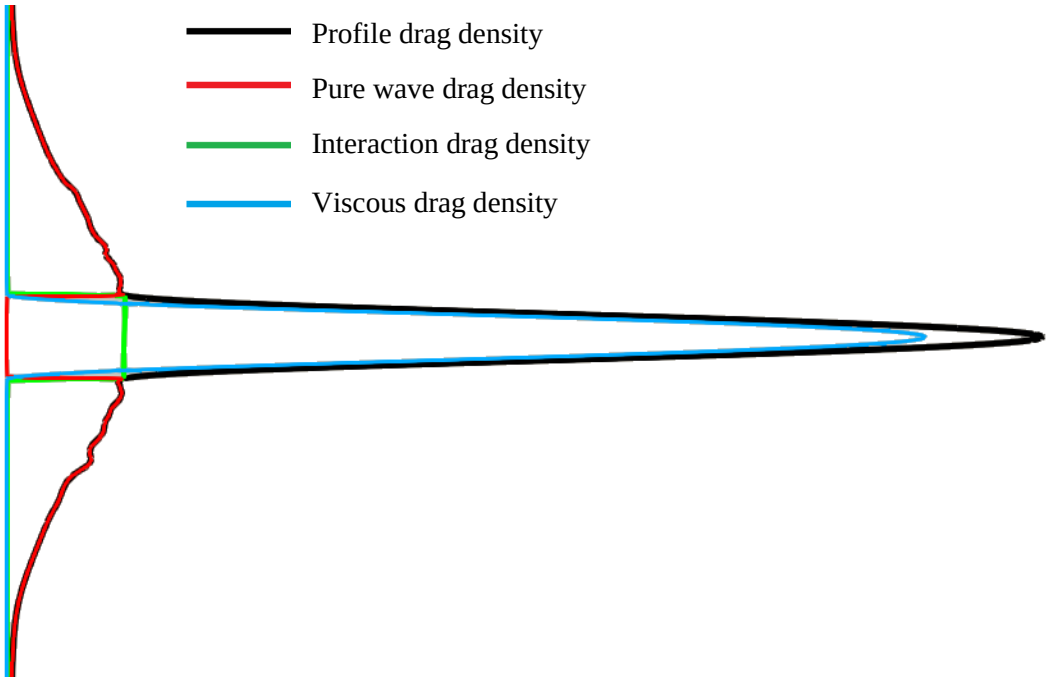

Fig. 22 Drag density distribution breakdown by Kusunose's technique

For this breakdown Kusunose has considered that the shockwave losses are propagated towards the airfoil's wall and thus, part of the total drag density peak region must also contains a part of this shockwave-boundary layer interaction. He proposed that shockwave losses are constant inside the boundary layer and equal to the pure shock drag value at the boundary layer end. Finally, the Kusunose's total wave drag is the sum of the pure wave drag and the interaction drag. That was already shown in Fig. 10.

However, by analyzing in detail the physics involved it is clear that shockwaves cannot exist on the subsonic region inside the boundary layer, thus no shock losses can occur there. The same conclusion is obtained while analyzing the integration domain used to calculate the shockwave anergy by the Arntz method [2]: this integration

volume lies outside the boundary layer, because it is based on the Lovely and Haimes shock detector [19]. Here is worth to mention that this shockwave detector criterion is used only to visualize the shockwave. However, the calculation of the wave anergy is done with the divergence approach shown in Eq. 16 by using a volume around the shockwave (equivalent to the addition of several mesh layers for its calculation by the flux approach [2]).

From this discussion it follows that the procedure proposed by Kusunose to extract the pure wave drag is correct. However, it is not correct to decompose the remaining part of the total profile drag into a pure viscous and an interaction part. In fact, the remaining part of the total profile drag is already the viscous drag, which of course, it takes into account the boundary layer thickening due to the shockwave impact and its related losses. By following this revised procedure, we obtain the Fig. 23, where the remaining part of the total profile drag (called here "viscous+ interaction" to retain the nomenclature of Kusunose) increases in the transonic region as expected (this was not the case in Fig.10). Moreover, the Fig. 23 is now comparable to the Fig. 12 (total anergy breakdown), where the viscous anergy increased in the transonic region.

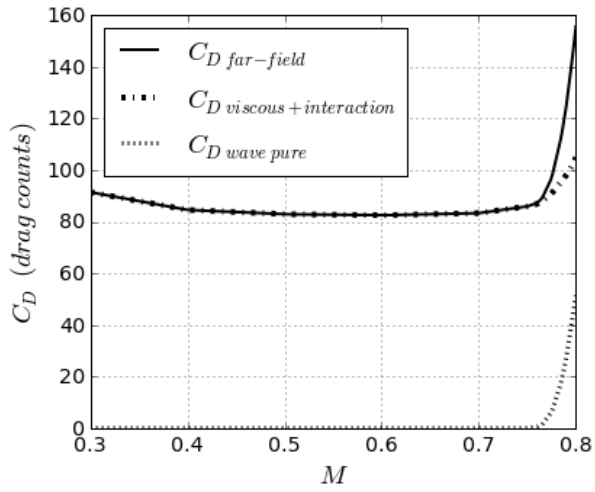

Fig. 23 Modified Kusunose's drag breakdown

B. Proposed method

The standard procedure recommended by Arntz to extract the wave anergy relies on a volume integral around the shockwave volume. This approach is affordable only for CFD analysis. If one intends to extract this anergy component from wind tunnel data it is simply impossible. That's why it is proposed to adapt the revised Kusunose's far-field decomposition technique to the exergetic analysis as follows. Firstly, the total anergy density profile is obtained along the survey line downstream of the body (Fig. 24). Then, a threshold value is used to delimit the extent of the losses attributed to the wave anergy (green zone). This is done by using the viscous anergy field (Fig.

25) simply because the anergy contributions that are not coming from the wave, are coming from the boundary layer. Finally, the total anergy profile can be splitted into its wave anergy region and the remaining one (containing the viscous and thermal anergies altogether) as shown in Fig. 26.

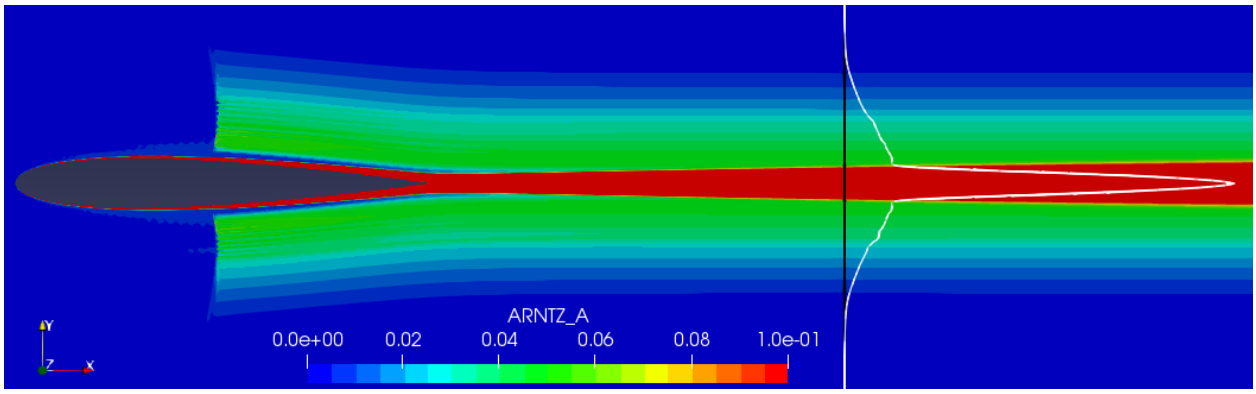

Fig. 24 Total anergy density field and its distribution along a survey line (M=0.85, α=0°)

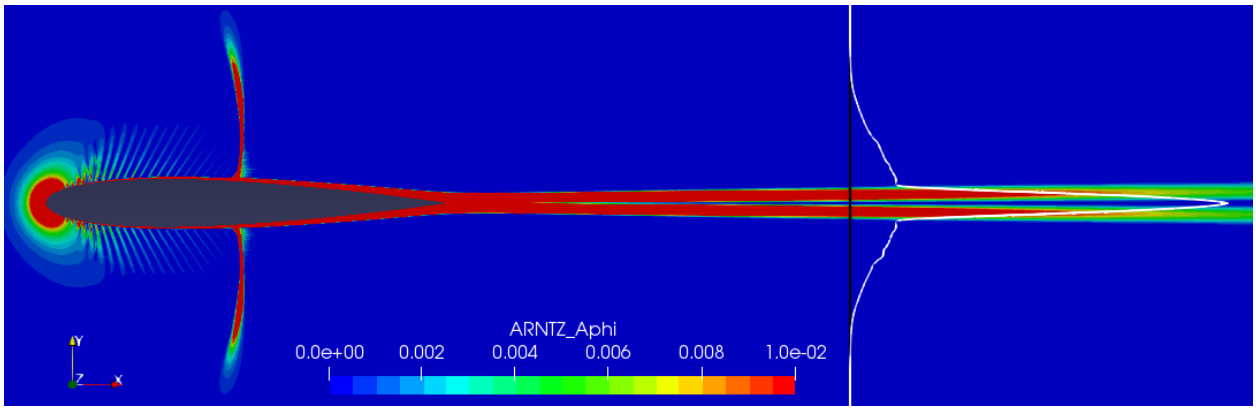

Fig. 25 Viscous anergy field and total anergy density distribution along survey line (M=0.85, α=0°)

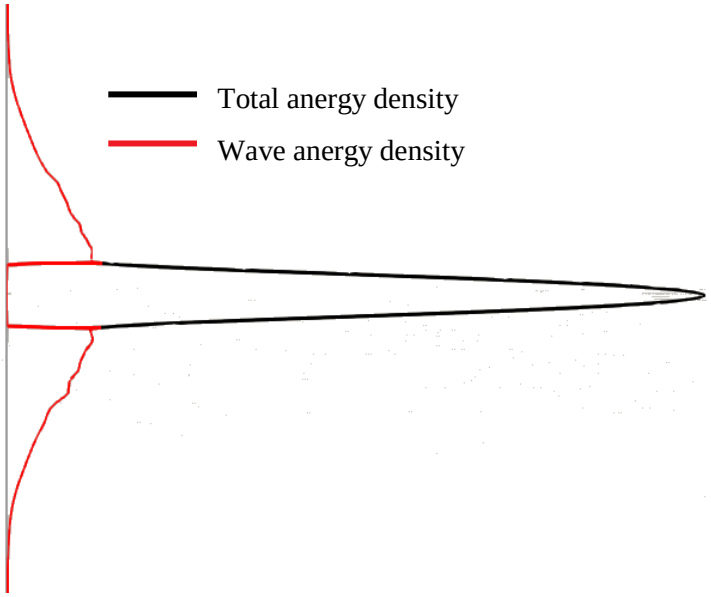

Fig. 26 Proposed far-field total anergy breakdown

Note: the scale of the Fig. 25 was chosen in order to discern the viscous region from the rest of the field. This also allows to see the viscous losses inside the shockwave region but they are negligible (about 2% of the total viscous anergy).

C. Results discussion

The wave anergy value extracted by several methods including the new one is shown in Fig. 27. The reference value here will be the wave anergy by the Arntz method because it is based on an exact analytical formulation and no hypotheses were done for its calculation. The pure wave drag by Kusunose technique was also added. This allows to confirm the pertinence of the correction to the Kusunose's method: the new wave drag value matches the exergy one, while the original approach adds the pure wave with the interaction component, leading to an over prediction of the total wave drag. Finally, the proposed far-field wave anergy extraction method (New method) is implemented for two survey plane positions: at the trailing edge of the airfoil (TE) and 1 chord downstream (1C).

It can be seen that the proposed method performs very well when the survey plane is at 1 chord but it over predicts the wave anergy value when the survey plane is at the trailing edge.

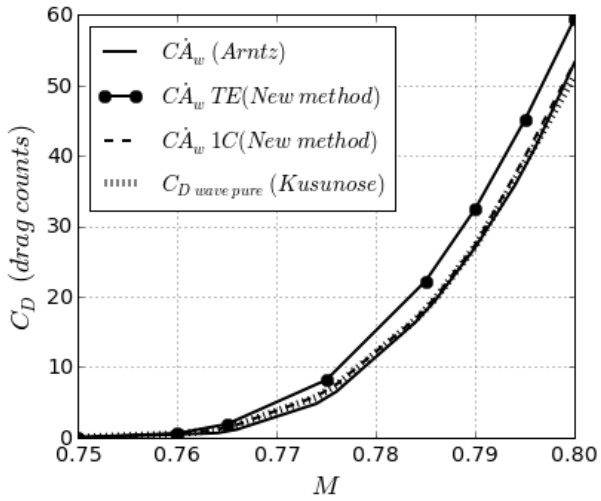

Fig. 27 Comparison of several wave anergy extraction methods

In order to further study this behavior, a survey plane sweep was done, by placing the plane at several positions downstream of the airfoil as shown in Fig. 28. It can be seen that when the survey plane is at least at 1 chord or downstream, the predicted wave anergy approximates very well the reference Arntz wave anergy value, with an error of less than 2 power counts. This is absolutely acceptable if we take into consideration that the typical measurement error of far field methods is about 5 % (which represents ±2.5dc for our case) [xx]. On the other hand, a limitation of the method is that the survey plane must not be placed more than 3 or 4 chords downstream of the airfoil because at that position is very difficult to stablish a valid threshold value for the viscous anergy. Moreover, the origin of the discrepancies for survey plane position very close to the airfoil is still under study: this is probably related to the potential effects.

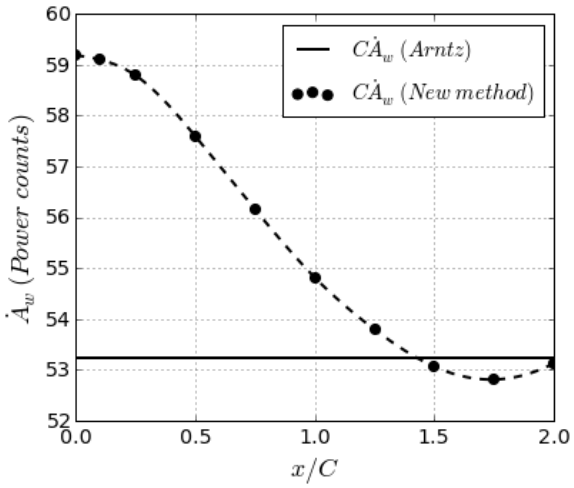

Fig. 28 Far-field wave anergy evaluated at several survey plane positions

VI. Conclusion

The present work has depicted the strong potential of the exergetic analysis to perform aerodynamic assessment of classical configurations: it has been shown that the Arntz method could provide exergetic-based characteristic curves for an airfoil and a wing as well (but not limited to these cases). The intuitive and easy to understand nature of its drag breakdown make this method an affordable tool for the flow analysis. Thus, this approach can be used to complement the classical near-field and far-field characteristic curves: the total amount of information provided by the 3 methods altogether allows a better physical understanding of the origins of airfoil and wing drag.

In addition, a new far-field wave anergy extraction method have been presented and validated against the classical approaches. This method will be especially useful for transonic wind tunnel tests where the total anergy and the wave anergy can be extracted by wake survey.

VII. Acknowledgments

The authors would like to thank ISAE-SUPAERO for supporting this research and Andy TURNBULL (SAFRAN TECH) for proofreading the paper. We would also like to show our gratitude to the reviewers for comments that greatly improved the manuscript.

VIII. References

[1] Drela, M., "Power Balance in Aerodynamic Flows," *AIAA journal*, Vol. 47, No. 7, 2009, pp. 1761-1771.
DOI: 10.2514/1.42409

[2] Arntz, A., "Civil Aircraft Aero-thermo-propulsive Performance Assessment by an Exergy Analysis of High-fidelity CFD-RANS Flow Solutions," Fluids mechanics, Université de Lille 1, 2014.
HAL Id: tel-01113135

[3] Hall, D., "Boundary Layer Ingestion Propulsion: Benefit, Challenges and Opportunities," 5th UTIAS International Workshop on Aviation and Climate Change, Toronto, Canada, 20th may 2016.

[x] Hayes, D., Lone, M., Whidborne, J. and Coetzee, E., "Evaluating the Rationale for Folding Wing Tips Comparing the Exergy and Breguet Approaches," 55th AIAA Aerospace Sciences Meeting, 9-13 January, Grapevine, Texas, USA, 2017.
https://doi.org/10.2514/6.2017-0464

[4] Drela, M., *Flight Vehicle Aerodynamics*, The MIT Press, Cambridge, MA, 2014 ISBN: 9780262526449.

[5] Anderson, J., *Fundamentals of Aerodynamics*, McGraw-Hill Education, Boston, 2010. ISBN 0073398101, 9780073398105.

[6] Betz, A., "A Method For The Direct Determination of Wing-Section Drag," NACA Technical Report 337, 1925.

[7] Jones, B., "Measurement of Profile Drag by the Pitot-Traverse Method," Aeronautical Research Council R&M Rept. 1688, 1936.

[8] Oswatitsch, K., *Gas Dynamics*, Academic Press, New York, 1956.

[9] Kusunose, A., "Extension of Wake-Survey Analysis Method to Cover Compressible Flows," *Journal Of Aircraft*, Vol. 39, No. 6, 2002, pp. 954-963.
https://doi.org/10.2514/2.3048

[10] Meheut, M., "Evaluation des Composantes Phénoménologiques de la Trainée d'un Avion à Partir des Résultats Expérimentaux," Thèse ONERA-Université des Sciences et technologies de Lille, France, 2006.

[11] Cengel, Y., Boles, M., *Thermodynamics: An Engineering Approach*, Eighth edition, Mc Graw Hill Education, New York, 2015.

[12] A.Bejan, *Advanced engineering Thermodynamics*, Second edition, John Wiley and Sons, New York, 1997.

[13] D. Riggins, Moorhouse, D., Camberos, J., "Characterization of Aerospace Vehicle Performance and Mission Analysis Using Thermodynamic Availability," *Journal of Aircraft*, Vol. 47, No. 3, 2010, pp. 904-9016.
https://doi.org/10.2514/1.46420

[14] Li, H., Stewart, J., Figliola, R., "Exergy Based Design Methodology For Airfoil Shape Optimization And Wing Analysis," 25th International Congress Of The Aeronautical Sciences ICAS, 3rd – 8th September, Germany, 2006.

[15] Alabi, K., Ladeinde, F., Spakovsky, M., Moorhouse, D. and Camberos, J., "The Use Of The 2nd Law As A Potential Design Tool For Aircraft Air Frame Subsystems," *International Journal of Thermodynamics*, Vol. 9 (No. 4), 2006, pp. 193-205. ISSN 13019724.

[16] Camberos, J. and Moorhouse, D., *Exergy Analysis and Design Optimization for Aerospace Vehicles and Systems*, Progress in Astronautics and Aeronautics, AIAA, 2011. eISBN: 978-1-60086-840-5

[xx] Hayes, H., Lone, M., Whidborne, J., Camberos, J. and Coetzee, E., *Adopting Exergy Analysis for use in Aerospace*, Progress in Aerospace Sciences, Volume 93, pp. 73-94, 2017.
DOI: 10.1016/j.paerosci.2017.07.004

[xx] Macian, F., Im, S., Garcia-Cozar, F. and Rao, A., *T-cell anergy*, Current Opinion in Immunology 2004, pp. 209–216
DOI 10.1016/j.coi.2004.01.013

[17] Aguirre, M. and Duplaa, S., "Exergetic drag prediction on the entire flight envelope of an airfoil and a wing," *International Journal of Exergy*, submitted for publication.

[xx] Smith, L., *Wake Ingestion Propulsion Benefit*, Journal Of Propulsion And Power Vol. 9, No. 1, pp.74-82, 1993.
https://doi.org/10.2514/3.11487

[18] Kusunose. A, Crowder, J., Watzlavick, Z., "Wave Drag Extraction from Profile Drag Based on a Wake-Integral Method," AIAA 99-0275, 37th AIAA Aerospace Sciences Meeting and Exhibit, January II-14, 1999. https://doi.org/10.2514/6.1999-275

[19] Lovely, D., Haimes, R., "Shock Detection From Computational Fluid Dynamics Results," *AIAA* 99-3285, 1999. https://doi.org/10.2514/6.1999-3285

[xx] AGARD, "Experimental Data Base For Computer Program Assessment," *AGARD Advisory Report No. 138*, 1979.